Supporting Information

Electrochemical PET recycling to formate through ethylene glycol oxidation on Ni-Co-S nanosheet arrays

Yi Ma,[ab] Luming Li,[a] Jialing Tang,[c] Zongkun Hu,[c] Yong Zhang,[ab] Ning Jian,[ab] Huan Ge,[ab] Jun Zhao,[d] Andreu Cabot,[ef*] Junshan Li[abe*]

a Institute for Advanced Study, Chengdu University, Chengdu 610106, China.

b School of Mechanical Engineering, Chengdu University, Chengdu, 610106, China.

c Department of Environmental Engineering, School of Architecture and Civil Engineering, Chengdu University, Chengdu, 610106, China

d Hebei Key Laboratory of Photoelectric Control on Surface and Interface, College of Science, Hebei University of Science and Technology, Shijiazhuang 050018, China

e Catalonia Institute for Energy Research - IREC, Sant Adrià de Besòs, Barcelona, 08930, Catalonia, Spain.

f ICREA, Pg. Lluís Companys 23, 08010 Barcelona, Catalonia, Spain.

SEM-EDS characterization

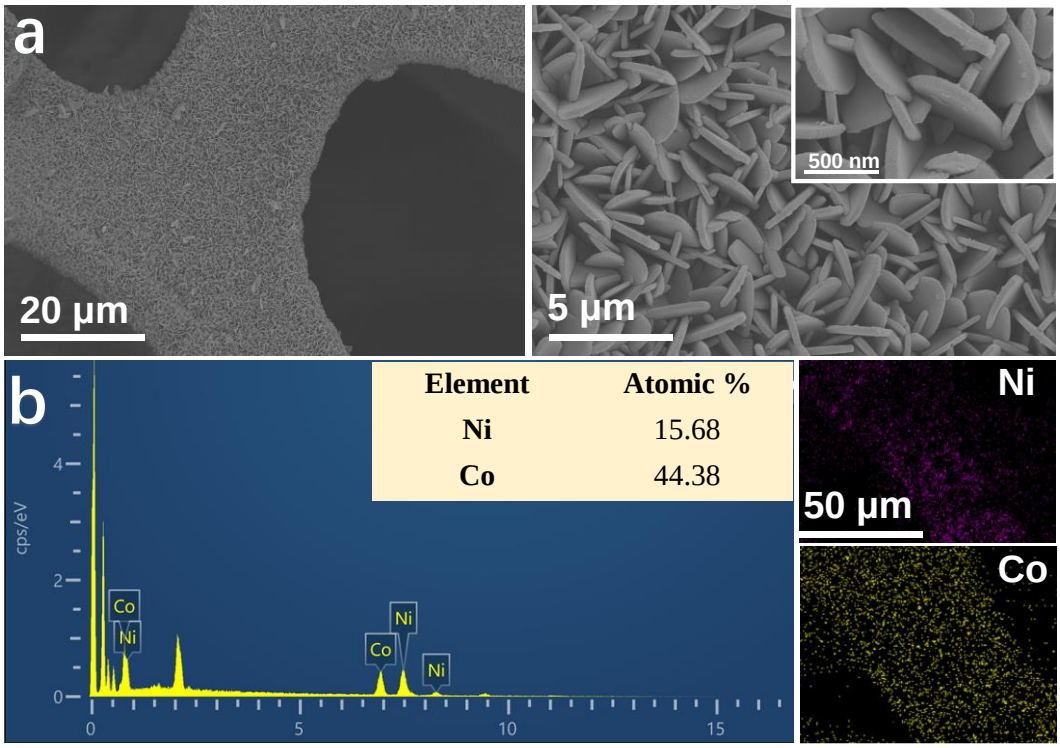

Figure S1. (a) Scanning electron microscopy image of Ni-Co NSAs/NF. (b) SEM-EDS measurement of Ni-Co NSAs/NF.

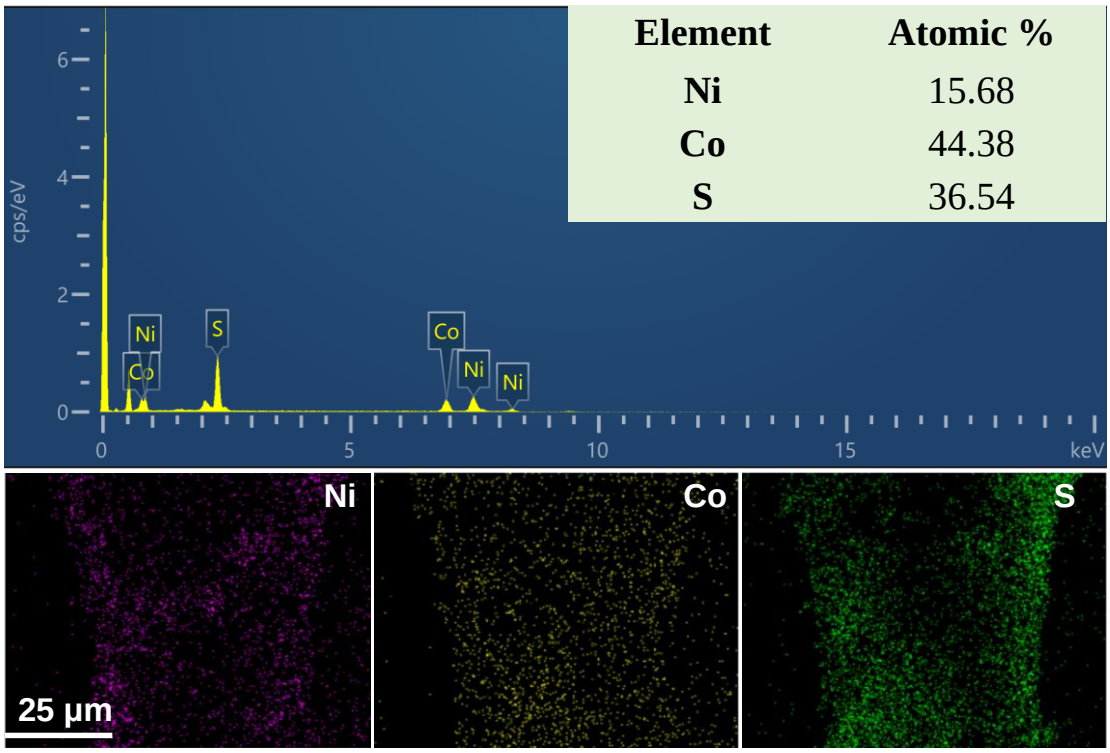

Figure S2. SEM-EDS measurement of Ni-Co-S NSAs/NF.

XPS spectra

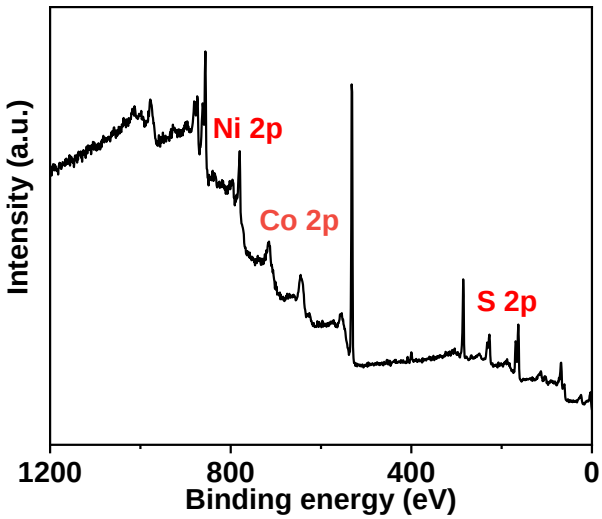

Figure S3. XPS spectrum for the Ni-Co-S NSAs/NF.

Electrochemical characterization

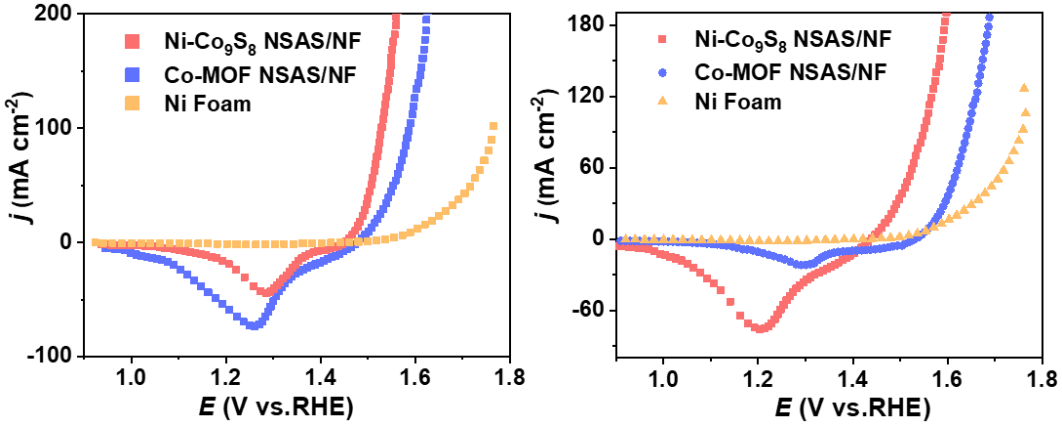

Figure S4. LSVs with iR correction of the NF, Co-MOF NSAs/NF, and Ni-Co_9S_8 NSAs/NF under 1 M KOH alkaline conditions (2nd Parallel measurement).

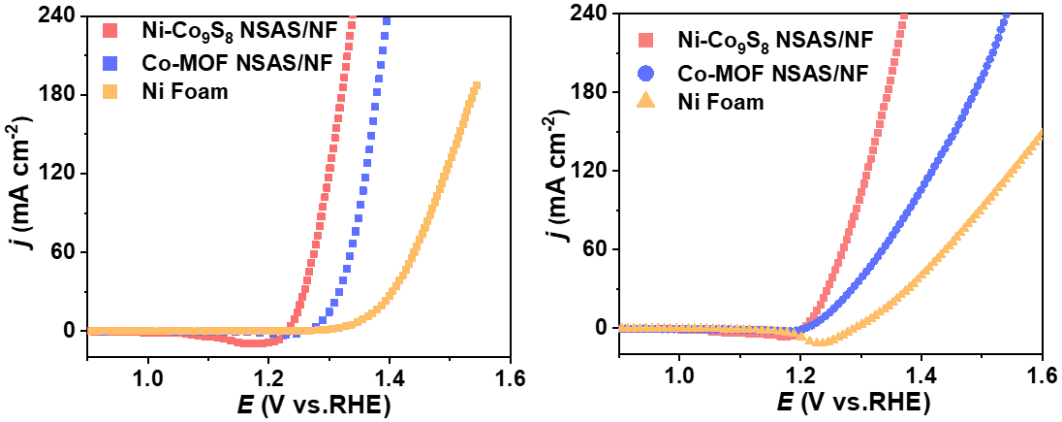

Figure S5. LSVs with iR correction of the NF, Co-MOF NSAs/NF, and Ni-Co_9S_8 NSAs/NF under 1 M KOH and 1 M EG conditions (3rd Parallel measurement).

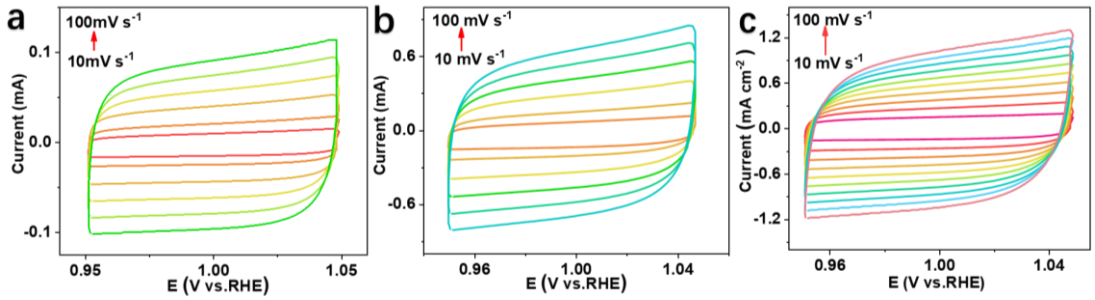

Figure S6. The CV curves of (a)NF, (b)Co-MOF NSAs/NF, and (c)Ni-Co_9S_8 NSAs/NF after 50 cycles at different scanning rates.

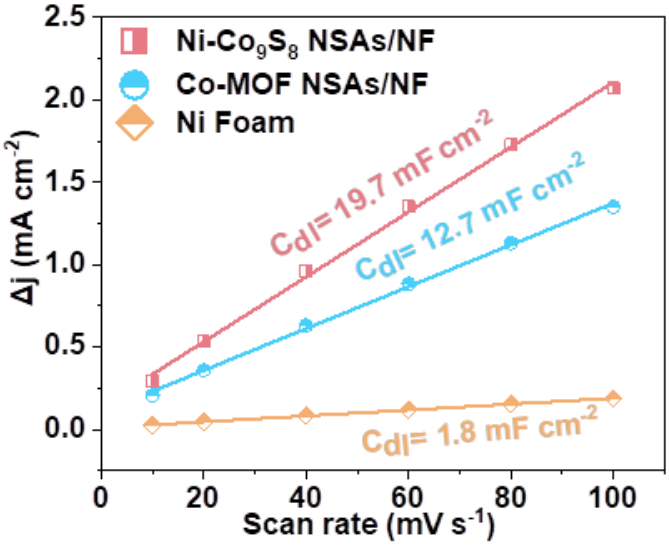

Figure S7. The calculated C_{dl} for the NF, Co-MOF NSAs/NF, and Ni-Co_9S_8 NSAs/NF based electrodes derived from Figure S4.

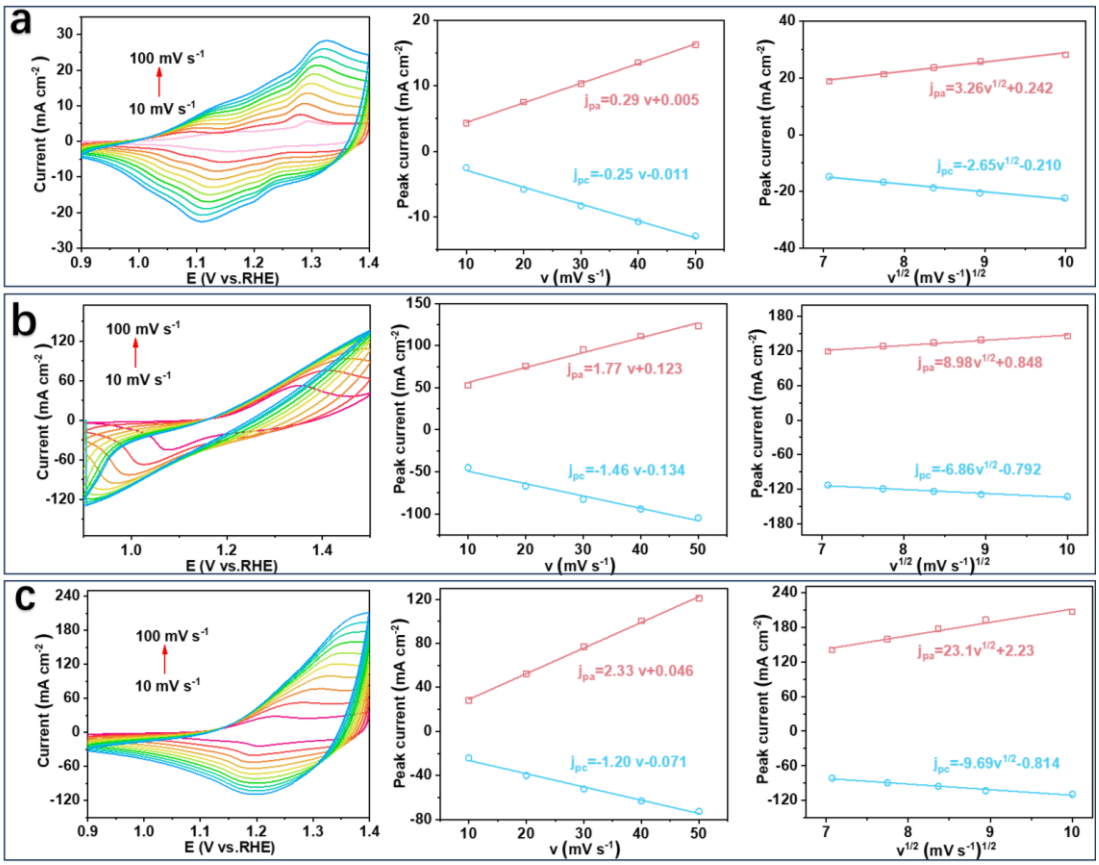

Fig S8. CVs with scanning rate from 10 to 100 mV s^{-1} in alkaline media, linear fitting of the anodic and cathodic peak current with the scanning rate, and linear fitting of the anodic and cathodic peak current with the square root of scanning rate for the (a)NF, (b)Co-MOF NSAs/NF, and (c)Ni-Co_9S_8 NSAs/NF based electrodes.

As shown in Fig. S8, when increasing the sweep rate, the position of the anodic peak shifted to higher potential values and the cathodic peak moved to lower potentials for four electrodes in 1.0 M. The current of both anodic and cathodic peaks rose linearly with increasing scan rate. From the average slope of the anodic and cathodic peaks vs. v, the surface coverage of redox species (Γ*) was estimated:

$$Ip = (n^2F^2/\ 4RT)A\Gamma^*v$$

where n, F, R, T and A are the number of transferred electrons (assumed to be 1), the Faraday constant (96485 C mol^{-1}), the gas constant (8.314 J K^{-1} mol^{-1}), temperature and the geometric surface area of the glassy carbon electrodes (0.196 cm^2), respectively.

Also, a linear relationship could be fitted to the dependence of the peak current density with the

square root of the voltage scanning rate for these four electrodes in 1 M KOH. This dependence is generally related with a diffusion-limited Ni $(OH)_2 \leftrightarrow$ NiOOH redox reaction, where the proton diffusion within the particle is considered the diffusion process that limits the reaction rate:

$$Ip = 2.69 \times 10^5 n^{3/2} A D^{1/2} C v^{1/2}$$

where I_p is the peak current, n is the number of transferred electrons, A is the geometric surface area of the GC, D is the diffusion coefficient, C is the proton concentration and was estimated to be 3.97 g cm^{-3}, we estimated at 0.043 mol cm^{-3}, and υ is the potential scan rate respectively.

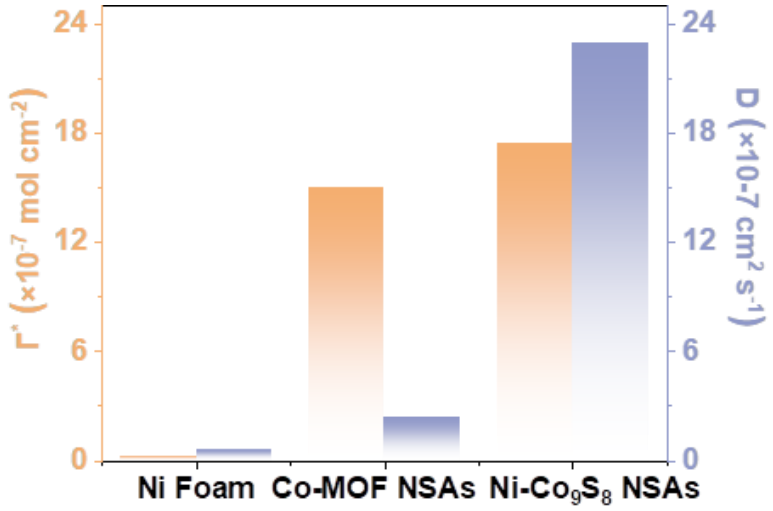

Figure S9. Surface coverage of redox species (Γ*) and diffusion coefficient (D) calculation for the NF, Co-MOF NSAs/NF, and Ni-Co_9S_8 NSAs/NF based electrodes.

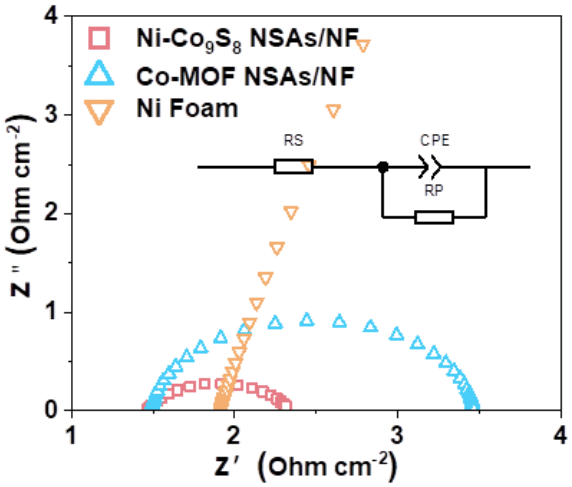

Figure S10. The Nyquist plots of the NF, Co-MOF NSAs/NF, and Ni-Co_9S_8 NSAs/NF based electrodes at 1.5 V vs. RHE in 1 M KOH containing 1 M EG.

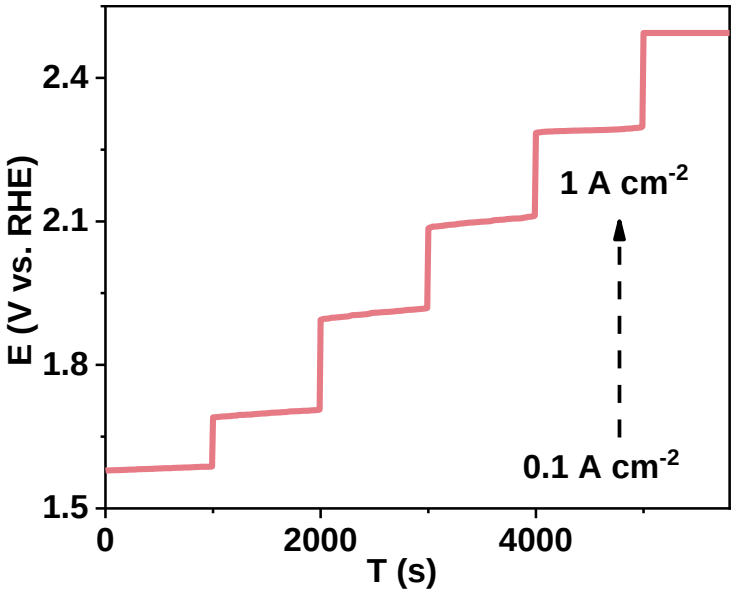

Figure S11. CP profile to generate a current density from 0.1 to 1.0 mA cm^{-2} for the Ni-Co_9S_8 NSAs/NF based electrode.

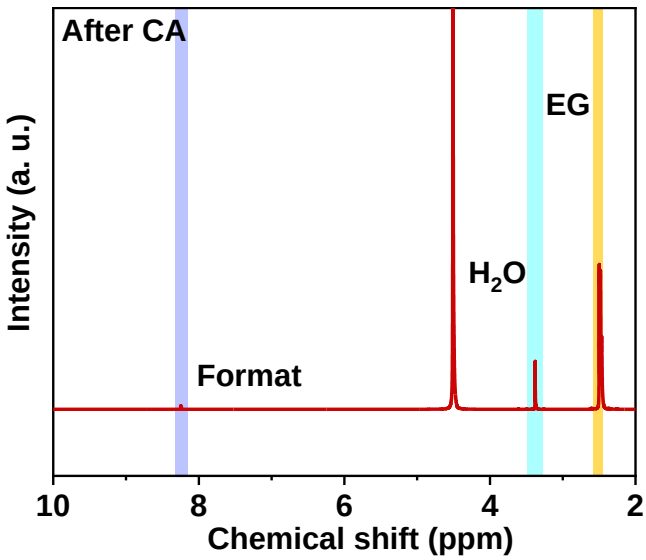

Figure S12. ^{1}H NMR spectra of electrolyte after 6 h CA test on Ni-Co_9S_8 NSAs/NF electrode.

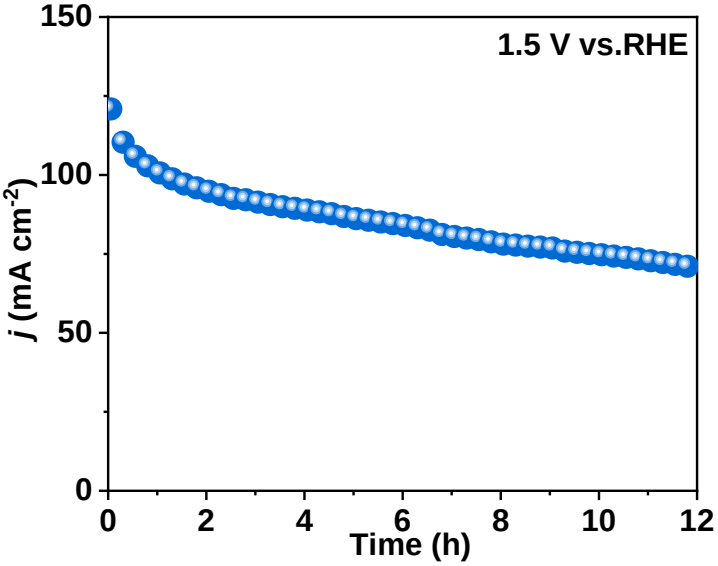

Figure S13. Another Long-term EGOR CA results at 1.5 V vs. RHE for the Ni-Co_9S_8 NSAs/NF electrode.

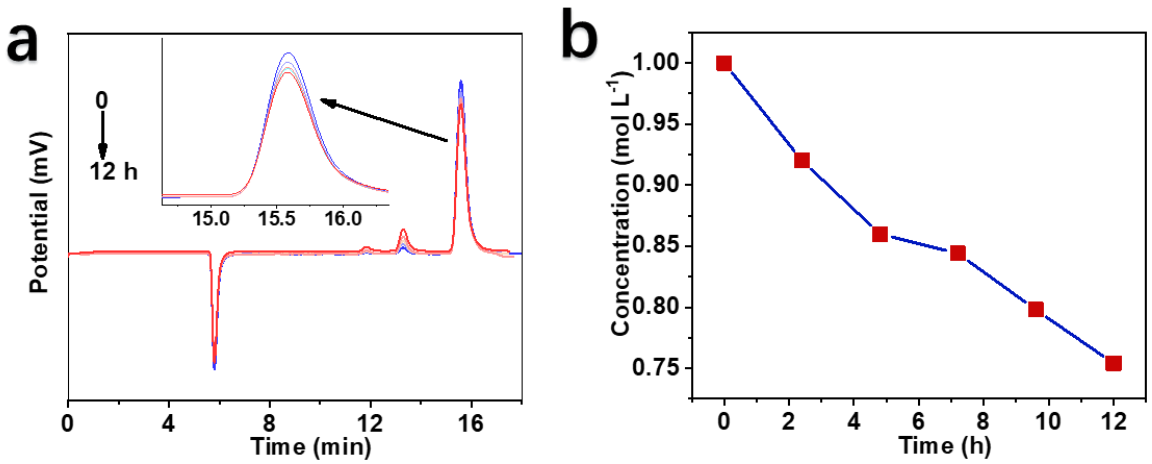

Figure S14. (a) Liquid phase detection plots of EG at different times in a continuous 12h CA test. (b) EG concentration obtained by labelling.

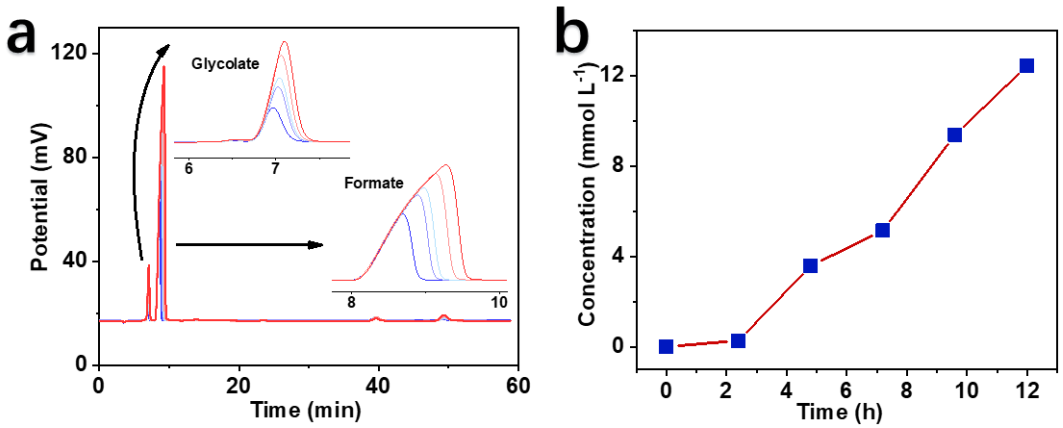

Figure S15. (a) Ion chromatographic detection plots at different times in the CA test and (b) concentrations detected by ethanoic acid.

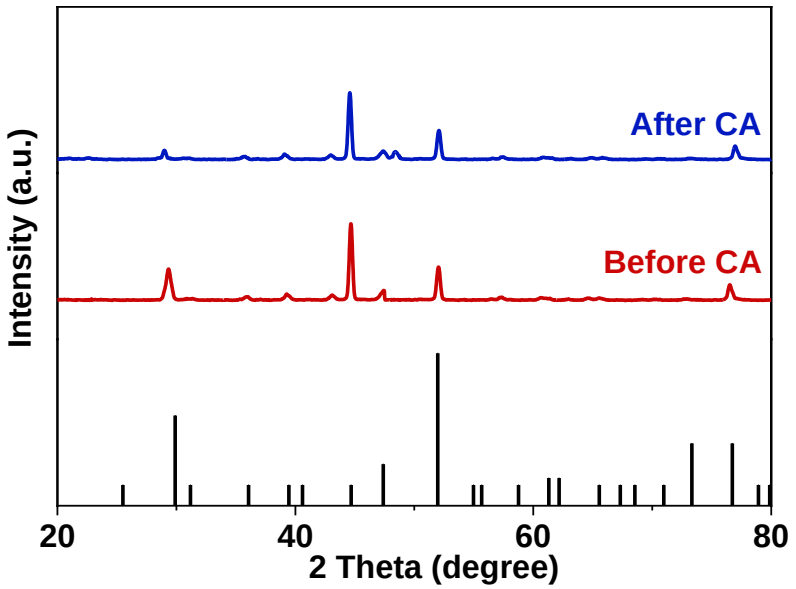

Figure S16. XRD patterns the spent Ni-Co_9S_8 NSAs/NF based electrode after 2 h and 12 h CA operation in 1 M KOH and 1 M EG.

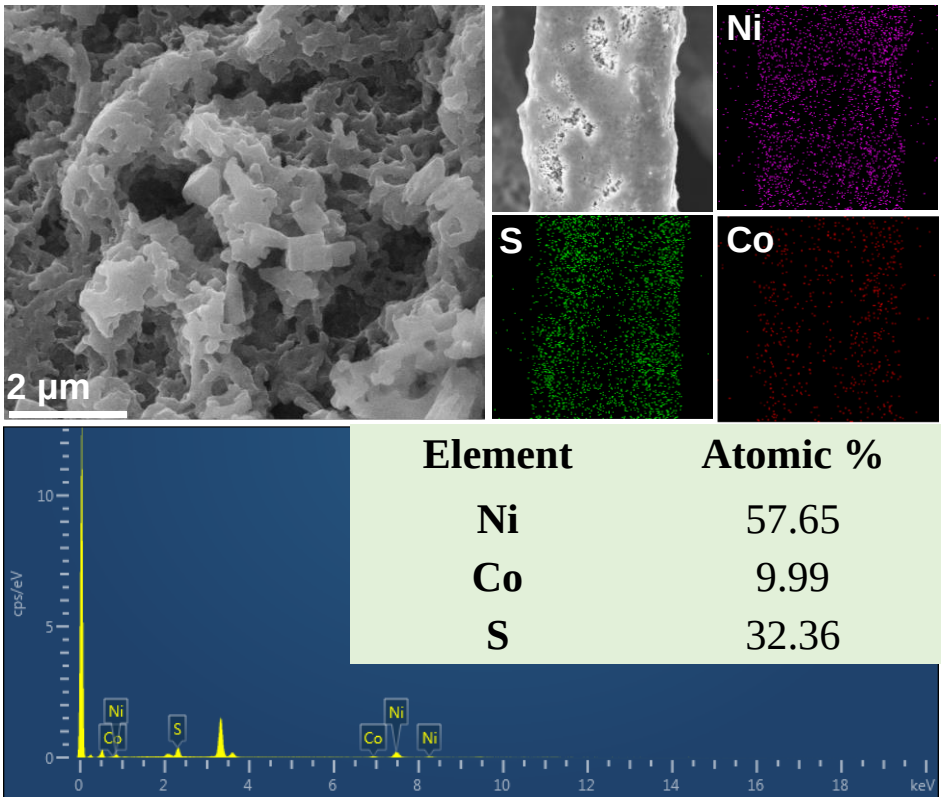

Figure S17. SEM images and SEM-EDS measurements of Ni-Co_9S_8 NSAs/NF based electrode after 2 h CA operation in 1 M KOH and 1 M EG.

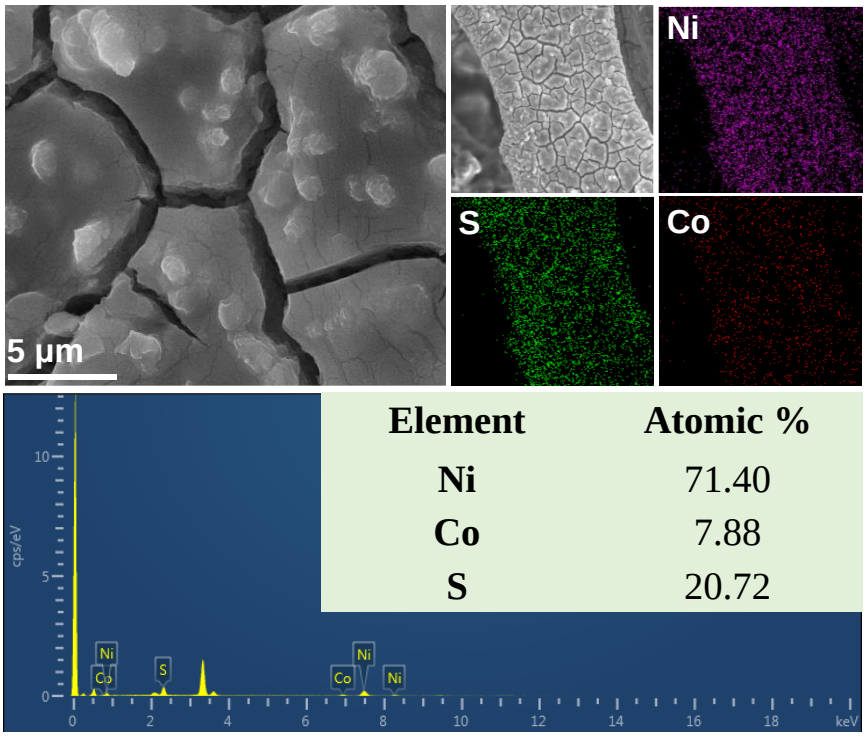

Figure S18. SEM images and SEM-EDS measurements of Ni-Co_9S_8 NSAs/NF based electrode after 12 h CA operation in 1 M KOH and 1 M EG.

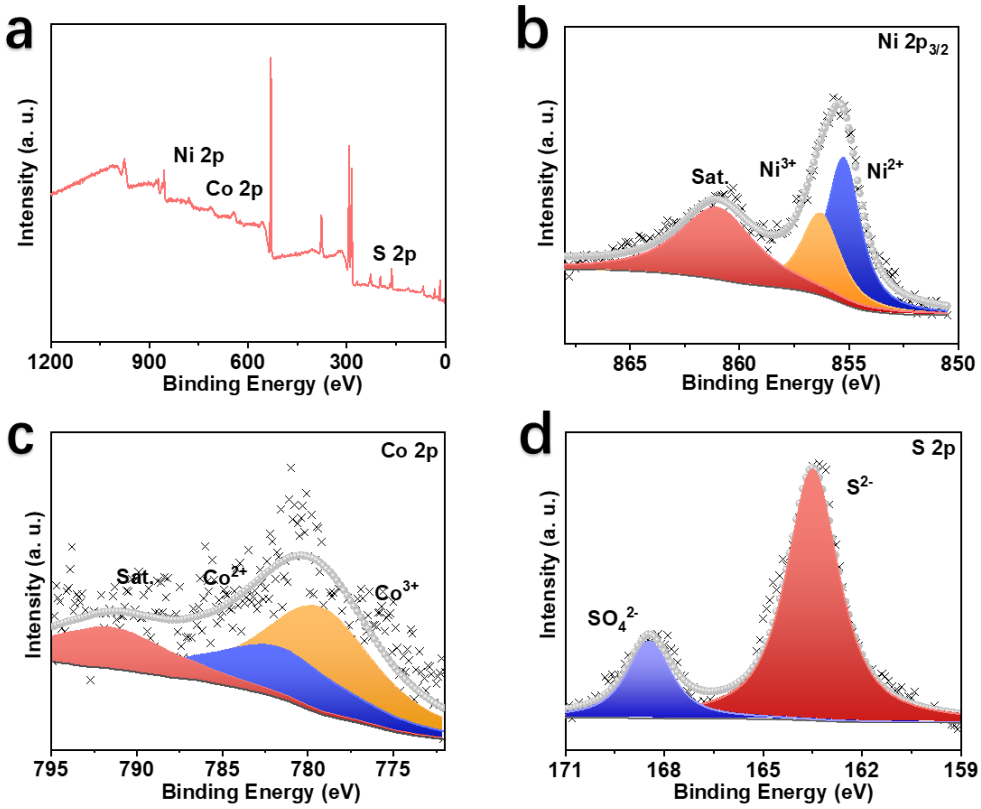

Figure S19. (a) XPS spectra and high-resolution (b) Ni $2p_{3/2}$, (c) Co $2p_{3/2}$ and (d) S 2p XPS spectra for Ni-Co_9S_8 NSAs/NF based electrode after 2 h CA operation in 1 M KOH and 1 M EG.

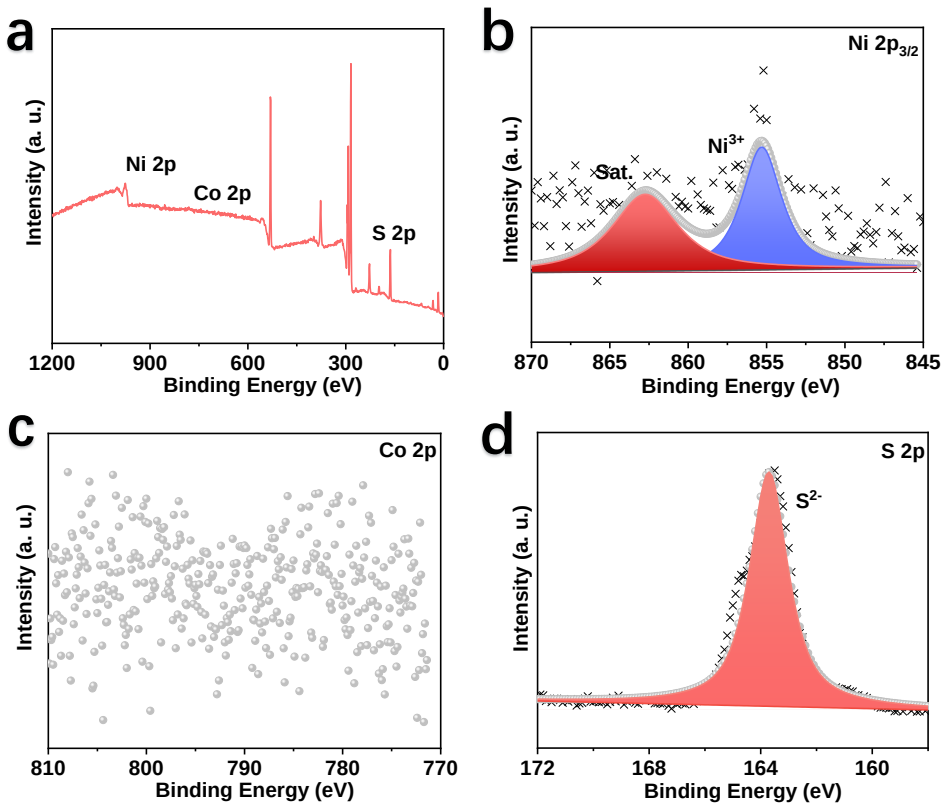

Figure S20. (a) XPS spectra and high-resolution (b) Ni $2p_{3/2}$, (c) Co $2p_{3/2}$ and (d) S 2p XPS spectra for Ni-Co_9S_8 NSAs/NF based electrode after 12 h CA operation in 1 M KOH and 1 M EG.

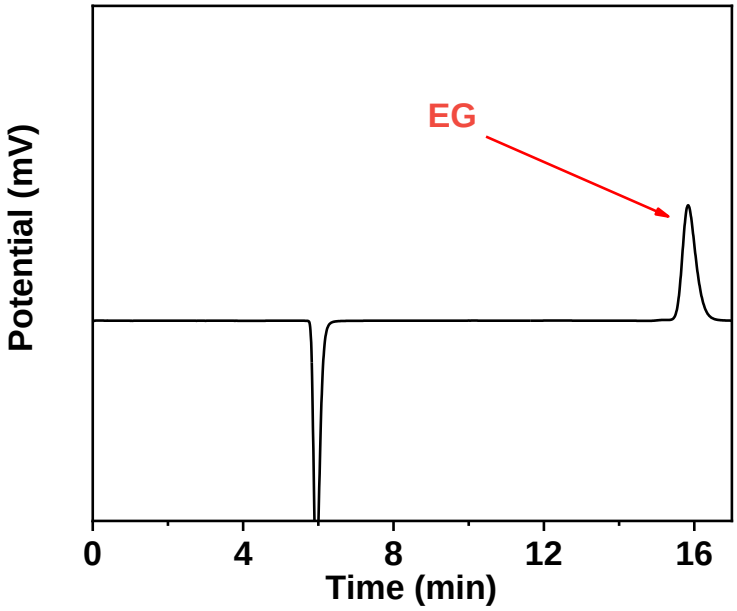

Figure S21. Standard EG profile for LC.

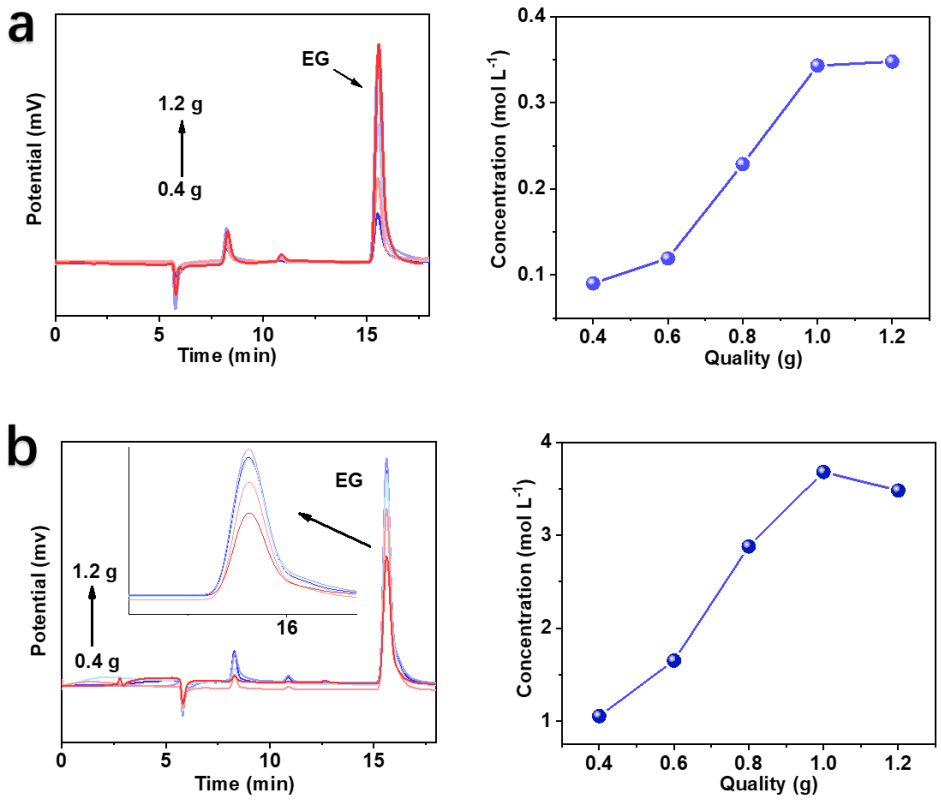

Figure S22. Another 2 parallel measurements for LC profile of PET hydrolysis products and EG yields for different amounts of PET hydrolysis.

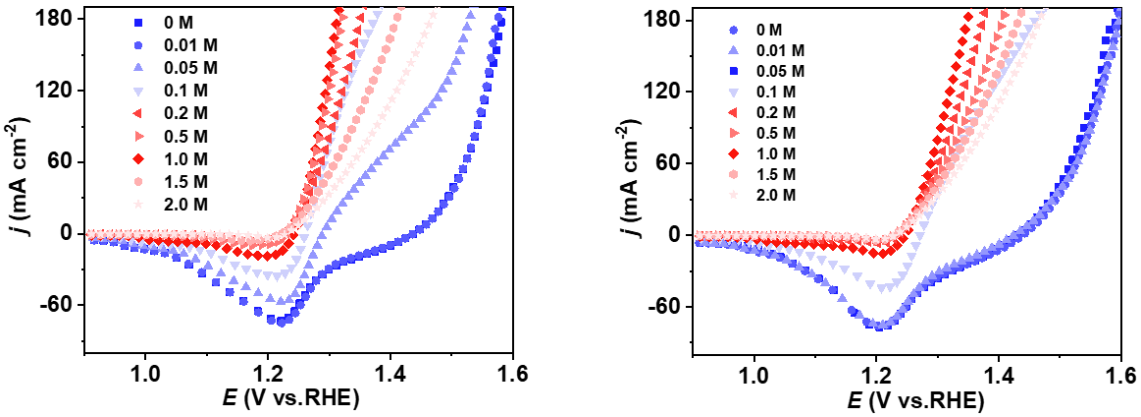

Figure S23. Another 2 parallel measurements for LSV curves with iR correction for Ni-Co_9S_8 NSAs/NF at different EG concentrations in 1 M KOH.

Table S1 Comparative Table of performances of different catalysts for ethylene glycol oxidation reaction in alkaline medium.

Catalyst	Current density ($mA\ cm^{-2}$)	Potential (V vs. RHE)	Electrolyte	Stability Decay (%) time	Main product and FE	Reference
Ni/WC NPs@C	68	1.6	1.0 M KOH + 1.0 M EG	n.a.	n.a.	[1]
$Ni(OH)_2$-NZB-MW/CPE	14	1.6	1.6 M NaOH + 0.14 M EG	35.7%@0.28h	n.a.	[2]
Ni NPs/ITO	1.6	1.6	0.2 M NaOH + 0.03 M EG	21%@0.8h	n.a.	[3]
FeCoNi/C	18	1.2	1.0 M KOH + 1.0 M EG	95%@0.14h	glycolate (~40%) oxalate (~40%)	[4]
$NiSe_2$/C	103	1.6	1.0 M KOH + 1 M EG	45.4%@10h	formate (83.4%) oxalate (5.4%) glycolate (7.4%)	[5]
rGO-NiMn	47.5	1.5	1.0 M KOH + 1 M EG	26.3%@2h	oxalate (n.a.)	[6]
Ni-Co Oxides	55	1.5	1 M KOH + 1 M EG	n.a	n.a.	[7]
$NiCu_{60s}$/NF	75	1.47	1 M KOH + 0.3 M EG	~33%@1h	formate(n.a.) glycolate(n.a.)	[8]
Co-Ni/CP	150	1.8	1 M KOH + 1 M EG	n.a@24h	glycolate (96.4%)	[9]
Ni-Co-S NSAs/NF	140	1.5	1 M KOH + 1 M EG	~40%@24h	formate(90%)	This work

Reference

[1] M. Zhang, J. Zhu, R. Wan, B. Liu, D. Zhang, C. Zhang, J. Wang, J. Niu, Synergistic Effect of Nickel Oxyhydroxide and Tungsten Carbide in Electrocatalytic Alcohol Oxidation, Chemistry of Materials 34 (2022) 959–969. https://doi.org/10.1021/acs.chemmater.1c02535.

[2] S. Eshagh-Nimvari, S. Karim Hassaninejad-Darzi, Synergistic effects of nanozeolite beta-MWCNTs on the electrocatalytic oxidation of ethylene glycol: Experimental design by response surface methodology, Materials Science and Engineering: B 268 (2021) 115125. https://doi.org/10.1016/j.mseb.2021.115125.

[3] Q. Lin, Y. Wei, W. Liu, Y. Yu, J. Hu, Electrocatalytic oxidation of ethylene glycol and glycerol on nickel ion implanted-modified indium tin oxide electrode, Int J Hydrogen Energy 42 (2017) 1403–1411. https://doi.org/10.1016/j.ijhydene.2016.10.011.

[4] T. Matsumoto, M. Sadakiyo, M.L. Ooi, T. Yamamoto, S. Matsumura, K. Kato, T. Takeguchi, N. Ozawa, M. Kubo, M. Yamauchi, Atomically mixed Fe-group nanoalloys: catalyst design for the selective electrooxidation of ethylene glycol to oxalic acid, Physical Chemistry Chemical Physics 17 (2015) 11359–11366. https://doi.org/10.1039/C5CP00954E.

[5] J. Li, L. Li, X. Ma, X. Han, C. Xing, X. Qi, R. He, J. Arbiol, H. Pan, J. Zhao, J. Deng, Y. Zhang, Y. Yang, A. Cabot, Selective Ethylene Glycol Oxidation to Formate on Nickel Selenide with Simultaneous Evolution of Hydrogen, Advanced Science 10 (2023). https://doi.org/10.1002/advs.202300841.

[6] S.S. Medany, M.A. Hefnawy, Nickel–cobalt oxides decorated Chitosan electrocatalyst for ethylene glycol oxidation, Surfaces and Interfaces 40 (2023) 103077. https://doi.org/10.1016/j.surfin.2023.103077.

[7] S. Sun, Y. Zhou, B. Hu, Q. Zhang, Z.J. Xu, Ethylene Glycol and Ethanol Oxidation on Spinel Ni-Co Oxides in Alkaline, J Electrochem Soc 163 (2016) H99–H104. https://doi.org/10.1149/2.0761602jes.

[8] H. Kang, D. He, X. Yan, B. Dao, N.B. Williams, G.I. Elliott, D. Streater, J. Nyakuchena, J. Huang, X. Pan, X. Xiao, J. Gu, Cu Promoted the Dynamic Evolution of Ni-Based Catalysts for Polyethylene Terephthalate Plastic Upcycling, ACS Catal 14 (2024) 5314–5325. https://doi.org/10.1021/acscatal.3c05509.

[9] Y. Lin, Y. Chen, H. Ren, Y. Sun, J. Chen, M. Wu, Z. Li, Inspiration of Bimetallic Peroxide for Controllable Electrooxidizing Ethylene Glycol Through Modulating Surficial Intermediates, Adv Funct Mater (2024). https://doi.org/10.1002/adfm.202404594.